Nuclear Instruments and Methods in Physics Research B28 (1987) 161–174
North-Holland, Amsterdam

THE ENERGY LOSS OF MEDIUM-ENERGY He^+ IONS BACKSCATTERED FROM A Cu(100) SURFACE

P.F.A. ALKEMADE, W.C. TURKENBURG and W.F. VAN DER WEG

Department of Atomic and Interface Physics, State University at Utrecht, P.O. Box 80000, 3508 TA Utrecht, The Netherlands

Received 19 January 1987 and in revised form 28 April 1987

A model is presented for the shape of the surface peak in the energy spectrum of backscattered ions in a channeling and blocking experiment. The elastic energy loss distribution of the ions is calculated by use of Monte Carlo simulation. The inelastic energy loss distribution is calculated by use of data obtained from gas phase ion–atom collisions. The model for the shape of the surface peak is applied to the analysis of energy spectra of 175 keV He^+ ions backscattered from a Cu(100) surface. It is found that, under channeling and blocking conditions, the inelastic energy loss in surface layers can be almost three times higher than under normal (i.e. random-incidence and -detection) conditions. It is therefore concluded that the inelastic energy loss depends strongly on the impact parameter of the collision.

1. Introduction

Slowing down of fast ions in solids has been a subject of study for many decades. As was shown already by Bohr in 1913 [1], slowing down or loss of kinetic energy is caused by elastic nuclear collisions and by interactions with electrons in the solid. A famous theoretical overview has been given by Bohr in 1948 [2]. The energy loss by elastic processes can in principle be calculated precisely. Its relative contribution to the stopping power (= average energy loss per unit of path length) is, however, almost negligible if the kinetic energy of, for example, He ions is above 25 keV. The inelastic processes, on the other hand, still lack a complete quantitative theoretical description. The model of Lindhard [3] (free-electron gas model) generally predicts quite well the electronic stopping power in terms of energy transfer from a charged particle to a plasma of free electrons. In the local-density approximation of the free-electron gas model of Lindhard [4], the (local) electronic loss is assumed to be a function of the local electron density and of the velocity and charge of the ion only. The stopping power is then obtained by an integration of the local energy loss over the volume of one atom in the solid. In 1967 Bonderup [5] applied the free-electron gas model in the local-density approximation and the Lenz–Jensen atom model to evaluate the electronic energy loss of protons in a solid. Ziegler [6] has used Hartree–Fock electron density functions in his comprehensive summary of the stopping power of ions in matter.

Under many different circumstances, however, deviations between the energy loss per unit of path length and the stopping power are observed or, at least, expected. Experiments about the stopping of fast ions in single-crystals indicate that the energy loss depends on the ion trajectory. For example, much attention has been given to the energy loss under planar or axial channeling conditions. Under these conditions ions will, on the average, not traverse the entire volume of the stopping medium with equal probability. Channeled ions traverse regions with low electron density in the midst of the channels and regions with high density near the walls. Therefore, the energy loss might deviate from the stopping power. Measured ratios for the energy loss in channeling directions and in random directions vary from almost unity [7] to a factor of 4 [8,9]. Trajectory dependence of the energy loss has been observed, for example, by van Loenen [10] in a so-called CHABLIS (CHAnneling and BLocking of Ions in Surfaces) experiment with medium-energy H^+ ions incident on a $NiSi_2$ layer grown upon a single-crystal of silicon. A higher as well as a lower energy loss along the crystal directions, compared with random directions, has been measured. Indications for a dependence of the energy loss on the ion trajectory, or impact parameter, have also been found in studies about the energy loss of ions transmitted through a foil as a function of the emergence angle. In some of these studies [11–13] a relationship between the emergence angle and average energy loss is observed which is explained by the impact-parameter dependence of the energy loss. Others [14,15], however, found that local variations in the foil thickness can fully account for the measured relationship. Furthermore, measurements of the energy loss in very thin foils have shown a decrease [16] as well as an

0168-583X/87/$03.50

increase [17] when the foil gets thinner.

In some recent experiments, using the technique of CHABLIS, relatively high energy losses of medium-energy, low-Z ions in the very surface of crystals have been reported [18,19]. These ions have interacted with a limited number of atoms in the solid only. Moreover, these interactions are not random but well selected. It is therefore expected that tabulated stopping powers [20] cannot be applied to calculate the energy loss of these ions. Such experiments may lead to a better understanding of the energy loss of ions in solids and reveal information about the impact-parameter dependence of the energy loss. This is true especially when the experiments are performed with a high-resolution analyzer [21].

An exponential dependence of the electronic energy loss on the impact parameter has been suggested by Oen and Robinson [22]. The impact-parameter dependence of the energy loss can also be derived [23] from the free-electron gas model of Lindhard [3,4] and other models [24,25]. According to calculations [24,23] the average energy loss of medium-energy, low-Z ions at small-impact parameters is about 1.5 times the stopping power.

In conclusion, there is still no conclusive theory nor experimental data for the impact parameter dependence of the electronic energy loss.

In this study we shall try to elucidate the question of the impact parameter dependence of the electronic energy loss. A description is given of an experiment in which a very high energy loss is observed for 175 keV He^+ ions in the surface layers of a Cu(100) crystal (sections 2 and 3). This experiment has been performed under channeling and blocking conditions (CHABLIS). In order to analyze the elastic and inelastic energy losses, a comparison is made between the shape of the surface peak in the energy spectra of backscattered He^+ ions as measured, and the shape of the surface peak as calculated by computer simulations. In our computer model the trajectories of ions in the crystal are simulated by a Monte Carlo procedure. Elastic and inelastic energy losses are calculated in all single ion–atom collisions along the paths of the ions through the crystal.

On the one hand, the Monte Carlo simulation provides, in section 4, relative backscattering probabilities in the various layers of the crystal as well as detection probabilities of the backscattered ions. On the other hand, the simulation is used in section 5 to calculate the effect of multiple scattering on the direction and energy of ions which are backscattered into the detector. Furthermore, inelastic energy losses are calculated in section 6, using a semiempirical formula for the energy transfer to electrons ejected in a single ion–atom collision. The formula has been derived by Rudd [26] in order to interpret energy spectra of electrons ejected in proton–atom collisions in the gas phase. Consequently, the influence of inelastic losses on the shape of the surface peak in energy spectra of the backscattered ions, is analyzed in section 7.

Our single-event approach is similar to that applied by Wilson et al. in their calculation of the energy straggling of MeV protons in gases [27]. Inelastic energy loss data obtained from ion–atom collisions in the gas phase, have been applied by Bierman et al. to calculate the stopping of noble-gas ions with kinetic energy of the order of 10 keV, in some metals [28].

A quantitative comparison (in section 8) of our simulation results with measured spectra reveals information about the average inelastic energy loss as well as the spread in energy loss of medium-energy, low-Z ions in small-impact parameter collisions.

2. Experimental

The measurements are performed in a UHV scattering chamber coupled to a 175 kV ion accelerator at the FOM Institute for Atomic and Molecular Physics in Amsterdam. A Cu(100) surface is cleaned by sputtering with a 700 eV Ar^+ beam (100 $\mu C/cm^2$) and subsequent annealing at 700 K. This procedure is repeated until – with AES – no carbon, oxygen and sulphur is detected and the (1×1) LEED pattern is observed. The clean copper crystal is bombarded with a 175 keV He^+ beam along the [110] crystal direction. Energy and angular distributions of backscattered He^+ ions are measured with a toroidal electrostatic analyzer, having an energy resolution (fwhm) of 0.4% and an angular resolution of 0.3°. The detection plane of the analyzer coincides with the (001) crystal plane. The energy spectra are recorded simultaneously at 64 scattering angles θ_s between 80° and 100°. The scattering geometry is shown in the insert of fig. 2.

The degree of neutralization of the backscattered particles is measured with a surface barrier detector and two deflection plates placed at a scattering angle of 90°. The degree of neutralization is determined by measuring the yield of backscattered particles with and without voltage on the plates. A neutralization fraction of 0.33 ± 0.02 is found. Measurements by Haight [29] of the charge state of He, backscattered from a silicium crystal, have shown that the neutralization is independent of the outgoing trajectory. Therefore, we assume that in our experiment the neutralization is also independent of the scattering angle and scattering layer. The fraction of backscattered He^{2+}, which is estimated to be not more than 0.04 [30], is neglected.

During the measurements the background pressure in the vacuum chamber is less than 10^{-8} Pa. The experiment is performed at room temperature. More details about the apparatus are given in refs. [31,32].

3. Channeling and blocking energy spectra

Three detection angles are selected for analysis: 83°, 90° (i.e. the blocking direction) and 97°, with respect to the incident beam. In order to reduce statistical fluctuations, nine spectra within an interval of 2.7° around each selected angle are added. Since small differences in kinematic factor within each interval would broaden the surface peak in the energy spectra, the original spectra are shifted in energy before the adding is performed. (Note that in our experiment a difference of +1° in the detection angle corresponds to a shift of the surface peak of −340 eV.) Due to a small systematical deviation in the curvature of the toroidal analyzer, a correction in the energy scale of the spectra as a function of the detection angle, has to be made. This correction has been determined independently [33] and varies from about −1 to +1 keV over the whole angular range of the analyzer.

Fig. 1 shows the surface peak of the three spectra after correction and summation. The dots represent the measurement. The meaning of the solid curves will be discussed later. In fact, the main part of this study will deal with the establishment of these curves. The width (fwhm) of the surface peak is 1.3, 1.0 and 1.2 keV at a detection angle of 83°, 90° and 97°, respectively. These values are significantly larger than the energy resolution of the analyzer, which is 0.6 keV.

When using the stopping power data of Ziegler and Biersack [20] the inelastic energy loss should not be more than 180 eV per crystal layer. Under our measuring conditions no more than about three atomic layers contribute to the surface peak in the energy spectra of backscattered ions. Therefore, one would not expect a peak width exceeding the energy resolution of the analyzer. Some broadening of the surface peak is caused by the presence of two copper isotopes, as will be discussed quantitatively in section 5. This effect, however, can still not explain the observed width of the peaks. Moreover, the three surface peaks differ in shape qualitatively; thus, the large widths cannot be explained in a simple way, for example by an unexpected poor resolution of the analyzer. We conclude that the surface peak is significantly wider than expected.

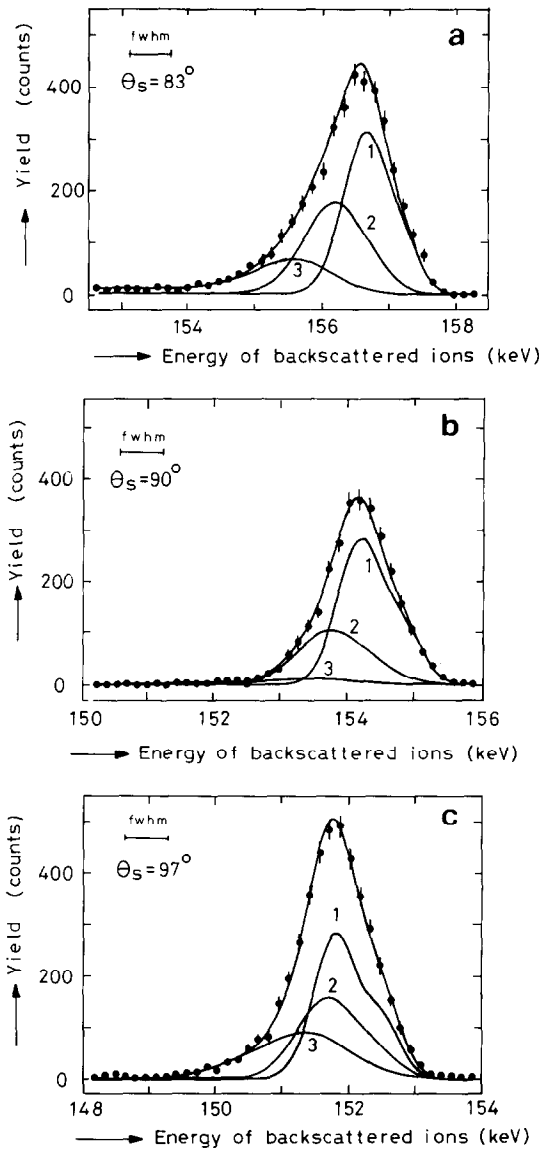

Fig. 1. Energy spectra of 175 keV He^+ ions backscattered from a Cu(100) surface. The indicated detection angles θ_s are relative to the direction of the primary beam. The dots represent the measured data, the solid curves are results of a fitting procedure based on our model for the shape of the surface peak. The calculated shape of the surface peak as well as the separate contributions from various crystal layers (1, 2, 3) are shown.

4. Monte Carlo simulation and the structure of the clean copper surface

In order to interpret the measured energy spectra, Monte Carlo simulations of the scattering process are performed. In the simulation a screened Molière potential to calculate scattering angles as a function of impact parameter and a 3-dimensional crystal model to calculate ion trajectories are used [19,23]. In ref. [19] we have used Monte Carlo simulations to determine the interlayer spacing at the surface and the thermal vibration amplitude of the atoms in the first and second crystal layer of the Cu(100) crystal. In a review paper by van der Veen [34], it is described how the structure of a crystal surface can be determined in a CHABLIS experiment in combination with results from Monte Carlo simulations. We have found [19] a contraction of the

Table 1
Normalized backscattering B_λ and detection D_λ probabilities as calculated for 175 keV He^+ ions incident along the [110] crystal axis of a clean Cu(100) crystal and scattered in the (001) detection plane. The relaxation of the first interlayer spacing has been taken -2% and the thermal vibration amplitude of atoms in the first and second layer 12 and 10 pm, respectively. The bulk value is 8.4 pm [36]. (Uncertainties are typically 0.02). The visibility V_λ is defined as $B_\lambda D_\lambda$

Layer	Backscattering probability	Detection probability at		
		83°	90°	97°
1	1.00	1.00	1.00	1.00
2	0.72	0.98	0.68	0.99
3	0.25	1.01	0.24	1.01
4	0.05	1.02	0.04	1.02
5	0.02	1.05	0.02	1.06
> 5	0.03	0.10	0.02	0.10

first interlayer spacing of -2% $\pm 2\%$ and a thermal vibration amplitude of 12 and 10 pm for the atoms in the first and the second crystal layer, respectively. These values are in good agreement with a dynamical LEED study by Davis et al. [35]. The bulk thermal vibration amplitude is 8.4 pm [36].

The calculated backscattering probability in the various surface layers as well as the detection probability of the backscattered ions are given in table 1.

5. Quantities determining the shape of the surface peak

The shape of the surface peak in the energy spectra is determined by physical and instrumental quantities such as ion energy, scattering and detection geometry, backscattering and detection probabilities, kinematic factor for the different isotopes, thermal vibration velocities of the target atoms, multiple scattering, inelastic energy losses (in, mainly, small-impact parameter collisions!), energy resolution of the accelerator and the analyzer. The influence of these quantities on the energy of the detected ions and therefore on the shape of the surface peak, will be discussed in this section. We shall focus our attention to the influence of kinematic factor differences, multiple scattering and inelastic energy loss. The inelastic energy loss of a He^+ ion in a copper crystal will be discussed in more detail in section 6.

5.1. Difference in kinematic factor

Copper consists of two isotopes: ^{63}Cu (69% abundance) and ^{65}Cu (31%). Because of their mass difference, the kinematic factors for He backscattered from these isotopes differ. The difference varies from 0.0031 at 83° to 0.0038 at 97° scattering angle. In our experiment this corresponds to 520 and 670 eV, respectively. As a result, the heavier, but less abundant ^{65}Cu isotope causes a tail at the higher energy side of the surface peak.

5.2. Shift and broadening of the surface peak by multiple scattering

The detected ions have obviously experienced at least one collision that causes a large-angle scattering. However, in many cases some small-angle scattering events may have occurred as well. These scattering events influence the direction and the energy of the backscattered ions and, consequently, the shape of the surface peak. In this section this influence is examined quantitatively by use of the Monte Carlo simulation.

The incoming beam is aligned along the [110] axis of the copper crystal (see the insert of fig. 2). This implies that ions, before they scatter over about 90° in the second or in a deeper layer, have to pass one or more atoms in the layer(s) nearer to the surface at a distance of typically a few tens of a picometer. As a result, one or more deflections occur with a scattering angle of the order of 1°. In our case the elastic energy loss in a scattering over about 1° is only 10 eV. Therefore, this influence on the shape of the surface peak can be neglected. However, double or multiple scattering causes also a discrepancy between the backscattering angle and the detection angle.

In fig. 2 some ion trajectories are shown that lead to detection of backscattered ions at an angle θ_s of 83°, 90° and 97°, respectively. It should be stressed that an atom in the second layer of the crystal can be hit by an ion only if, due to thermal vibration, this atom is located momentarily in or just outside the edge of the shadow cone of the atom in the first surface layer. Because of the Gaussianlike distribution of the thermal displacements, a position far outside the shadow cone is very unlikely. Therefore, in our scattering geometry the distance at which an ion passes a first-layer atom before it hits an atom in the second layer is confined to a limited range. If the passage distance is too small, the ion is deflected such that it will pass with a high probability the second-layer atom at a large distance. In that case scattering by the second-layer atom over about 90° cannot occur. On the other hand, if the passage distance in the first layer is too large, the passage distance in the second layer will probably be too large as well. Hence, only a passage distance in the first layer close to 20 pm, and consequently a small-angle scattering (over about 1.5°), can lead, with a relatively high probability, to backscattering in the second layer. The small-angle scattering may be positive or negative. Moreover, it may be within the detection plane (as is shown in fig. 2) or perpendicular to that plane. Note furthermore that the projection of the deflected trajectory onto the detection plane can have any value between about $-1.5°$ and $+1.5°$.

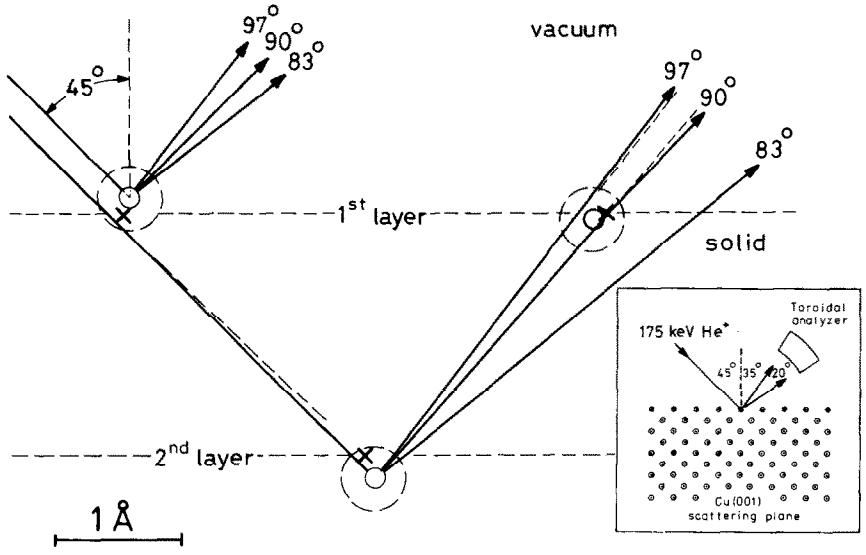

Fig. 2. Some ion trajectories which lead to the detection of an ion in the analyzer at a detection angle $\theta_s = 83°$, 90° and 97°, respectively. The insert shows the geometry of the experiment. The radii of the L- and M-shells of the Cu atoms are shown by circles. Note that the atoms are temporarily displaced from their equilibrium positions (indicated by ×), making backscattering in the second layer and detection at 90°, i.e. the blocking direction, possible. In all collisions elastic and inelastic energy losses occur.

Assuming double scattering only, a small deflection of δ_θ within the detection plane naturally implies that backscattering over $\theta_s - \delta_\theta$ is needed in the second layer to detect the ion at angle θ_s of the analyzer. So, double or multiple scattering causes a spread in the backscattering angle of the ions. Because of the angular dependence of the kinematic factor, a spread in the scattering angle corresponds to a spread (of 340 eV per degree, see section 3) in the energy of the detected ions.

Of course, small-angle scattering can occur also after backscattering in the second or a deeper layer. Apart from a spread, multiple scattering can cause also a shift in the average direction of the detected ions. For instance, ions which are backscattered over 83° in the second layer, will, on the average, be deflected in a following passage of a first-layer atom towards a lower detection angle (see fig. 2). On the other hand, ions which are backscattered over 97° will be deflected, on the average, to a higher detection angle. Thus, the mean detection angle of the ions backscattered in the second or in a deeper layer, differs more from 90° than the backscattering angle does. Therefore, at those detection angles there is a difference in mean kinematic factor between ions backscattered from the first layer, which are not affected by multiple scattering, and ions backscattered from a deeper layer, which are necessarily affected by multiple scattering. Consequently, a net shift in the energy of the ions backscattered from the surface layers will be measured at detection angles of 83° and 97°. At a detection angle of 90°, only a spread and no shift in energy will be found.

The average impact parameter, the deflection angle of the ions and the corresponding spread and shift in the energy of the detected ions are calculated by use of the Monte Carlo computer simulation model. Table 2 summarizes the results. It can be seen that in our experiment the energy distribution of the ions backscattered in the second layer may be shifted by about 190 eV and broadened by about 450 eV. Obviously, the energy distributions of the ions which are backscattered in the third or deeper layers are shifted and broadened, too. The shift and broadening of the latter distributions are, according to Monte Carlo calculations, a few tens

Table 2
The effect of multiple scattering on the energy of the detected ions, as calculated with Monte Carlo simulation. Indicated are the average distance at which ions pass atoms in the first layer assuming backscattering in the second layer, the corresponding average deflection angle and its spread (standard deviation), as well as the shift $\overline{\Delta E}_m$ and spread σ_m in the energy of these ions

	Path of the ions			
	Incoming	Outgoing		
Detection angle θ_s:	–	83°	90°	97°
Average impact parameter (pm)	15	30	15	30
Deflection (deg)				
average	0.1	−0.5	0.1	0.5
spread	0.8	0.7	0.8	0.7
Change in energy (eV)				
shift	20	−170	20	170
spread	300	200	350	200

of a percent higher than those for the second layer. The visibility, i.e. the backscattering probability times the detection probability (see table 1), of deeper layers, however, is small and these figures have therefore not been included in table 2.

5.3. Inelastic energy losses

As argued in the introduction, we cannot apply usual formulas [37] and data [20] for the stopping power or the energy straggling to calculate the inelastic energy loss of ions which are backscattered in different crystal layers. Instead we shall describe the interaction of ions with the copper crystal in terms of series of ion–atom collisions. The interaction of fast ions with atoms in the gas phase has been studied extensively [38]. We assume that results from such studies can also be applied to describe the interaction of fast ions with atoms in a crystal.

In a collision between a fast He ion and a relatively heavy target atom, kinetic energy of the ion may be lost inelastically by excitation and/or ionization of (mainly) the target atoms. The total amount of inelastic energy loss of an ion when moving through a crystal, is determined by the total number of excited and ejected electrons, their excitation of binding energy and the final kinetic energy of the ejected electrons. The number of electrons involved depends on the excitation and ejection probability and the number of collisions at various impact parameters. This number depends on the trajectory of the ion in the crystal.

Furthermore, energy is lost continuously in distant collisions by polarization of the medium in which the ion moves [2]. According to the equipartition rule [39], the continuous energy loss is equal to the average electronic energy loss in close collisions and, consequently, half the electronic stopping power.

Experimental data about the inelastic energy loss in atomic collisions are abundant for inert gases and gases like H_2, N_2, CO and O_2 (see, for example, refs. [40,41]). On the other hand, energy loss data for collisions of He ions in atomic vapours of copper (or equivalent) metals are hardly available. Therefore, the required information has to be derived from extrapolation of data acquired from the gases mentioned above. Alternatively, it can be derived from theoretical models for direct Coulomb ionization, such as the plane-wave-Born approximation (PWBA) [42], the classical binary-encounter approximation (BEA) [43] or the semiclassical approximation (SCA) [44], or from models for the molecular promotion mechanism [45].

Table 3 gives estimations for the ionization cross sections and probabilities for 175 keV He^+ as a function of the (sub)shell of copper atoms in the gas phase. Note that the velocity of the ions, 2.9×10^8 cm/s, is less than, for example, the average velocity of the electrons is the 3p-subshell (5.4×10^8 cm/s). This implies that theoretical models, such as PWBA or BEA, to calculate cross sections for excitation and ionization of electrons from these subshells are of limited validity. At much lower ion velocities, calculations could be performed by regarding the collision pair as a quasimolecular system [45].

Ion–atom collision experiments [48] and theoretical models (for example BEA [49]) reveal that the ionization probability depends on the impact parameter. The probability is roughly constant for impact parameters smaller than the shell radius r, and zero for impact parameters larger than this radius. Therefore, the overall ionization probability P, presented in table 3 (last

Table 3
The subshells of copper, their binding energies and cross-sections for ionization by impact of 175 keV He^+ in atomic Cu vapour. Ionization probability P per electron is defined as $\sigma/N\pi r^2$

Shell	Binding energy I (eV) [a]	Shell radius r (pm)	Number of electrons N	Ionization cross section σ (pm^2)	Ejection probability $P \equiv \sigma/N\pi r^2$
1s	8985	1.8	2	6×10^{-10} [b]	3×10^{-11}
2s	1105	9	2	1×10^{-2} [b]	2×10^{-5}
2p	950	9	6	4×10^{-2} [b]	3×10^{-5}
3s	129	26	2	2×10^{2} [c]	0.05
3p	83	26	6	2.2×10^{3} [c]	0.17
3d	11	~60	10	3×10^{4} [d]	0.2
4s	8	~100	1		

[a] From ref. [45].
[b] From [46].
[c] These figures are estimations using eq. (6) (section 6.3) and an effective charge number $Z_e = 2$ of the He^+ ion and a cutoff distance b_m of 26 pm, equal to the mean radius r_μ of the 3s- and 3p-subshell.
[d] These figures are estimations based on data for inert gases and H_2, N_2, CO, CH_4, CO_2 and O_2 [40,41] and a semiempirical model [26].
All figures for cross-sections and probabilities have an uncertainty of at most a factor of 2.

column), has been calculated by dividing the cross section by $N\pi r^2$, in which N is the number of electrons in the subshell. It roughly indicates the probability for a given electron in the considered subshell to be ejected in a small-impact parameter collision (i.e. $b < r$). The average kinetic energy of an ejected electron is comparable to the binding energy [26]. For Cu atoms, ionization or excitation of K- and L-shell electrons by impact of 175 keV He^+ ions is very unlikely. On the other hand, ionization of at least one 3d- or 4s-electron is very probable, as shown in table 3, but the energy loss involved (about twice the binding energy) is small. The cross section for multiple ionization of, for example, Ar by 40 keV H^+ impact [50], is considerably smaller than for single or double ionization. Therefore, we assume that, on the average, two electrons from the 3d- and 4s-subshells are ejected per He + Cu collision. The energy loss involved is estimated to range from 20 to 80 eV.

Generally, at impact energies above 10 keV/amu, the cross section for excitation to bound levels [38] and therefore the energy loss caused by excitation are lower than that for ionization. Moreover, less energy is involved [51]. We estimate that in our experiment the average energy loss by (single- or multiple-) excitation to bound levels of Cu ranges from 10 to 40 eV per collision.

Table 4 summarizes the estimated average energy loss and the spread in small-impact parameter ($b < 26$ pm, see section 6.1) collisions of a 175 keV He^+ ion with a Cu atom in a solid for the various inelastic processes. The total average inelastic energy loss is about 285 eV, the spread is about 155 eV *. It is concluded that most energy is lost by ionization of 3s- and 3p-electrons, on the average about 165 eV. The energy loss in distant collisions (i.e. by polarization of the medium) is about equal to half the electronic stopping power [2,39], i.e. 180 eV/nm [20]. When we take the size of an atom equal to the interatomic distance in a copper crystal (256 pm), this loss corresponds to 45 eV per collision.

It should be noted that kinetic energy of the ion is also lost when it captures an electron. However, neutralized He cannot be detected with an electrostatic analyzer as used in our experiment. Moreover, at the velocity involved, the cross section for electron capture is almost two times smaller than for ionization [40,41,51].

* In a copper solid the binding energies are, with respect to the Fermi-level, about 6 eV lower. Therefore, differences of about 10% in the average energy loss between the gas phase and the solid state can occur.

Table 4
Estimated average and spread of the inelastic energy loss of 175 keV He^+ ions due to ionization and excitation in small-impact parameter collisions with Cu atoms in a solid and the unlocalized loss by polarization of the medium. The uncertainty in the figures is about 25%

	Average energy loss per collision (eV)	Spread (eV)
Ionization		
1s	$\sim 10^{-6}$	0.1
2s	0.1	10
2p	0.3	20
3s	25	75
3p	140	125
3d + 4s	50	35
Excitation	25	25
Polarization	45	0
Total	285	155

6. Energy loss distribution of the detected ions

The inelastic energy loss of a He^+ ion in a copper crystal will be analyzed in more detail and a distribution of the inelastic energy loss of the detected ions is derived. As stated before, the interaction of an ion with atoms of the crystal is considered as a series of isolated ion–atom collisions. Consequently, the total inelastic energy loss of the ion can be regarded as the sum of the individual losses in all collisions plus the loss by polarization of the medium.

We start with a semiempirical probability distribution for a specific energy transfer to an ejected electron in a small-impact parameter collision. Subsequently, we derive the probability distribution for an energy transfer to all electrons ejected in one collision. Finally, the distribution of the energy transfer in more than one small-impact parameter collision is derived. Since the ion trajectories, calculated in the Monte Carlo simulation, are known, also the number of small-impact parameter collisions is known. From this number the energy loss distribution of the detected ions can be calculated.

6.1. Definitions

We define a passage of an ion along an atom as a *collision* if the impact parameter is smaller than half the interatomic distance of the crystal (128 pm for copper). A collision is called a *small-impact parameter collision* if the impact parameter is comparable to or smaller than the radius of the 3s- or 3p-subshell (26 pm). If the scattering angle is more than about 90°, the collision is called a *backscattering collision*. It is noted that a 175 keV He ion is backscattered from a copper atom only if

the impact parameter is smaller than about 0.3 pm. The number of collisions of an ion with atoms during its passage through the crystal will be denoted by n_C; the number of small-impact parameter collisions by n_S.

6.2. Differential ionization cross section

A semiempirical formula for the differential cross section $\sigma_j(T, \Delta E)$ for the ejection of electrons from subshell j with kinetic energy ΔE in a proton–atom collision in the gas phase has been given by Rudd [26]:

$$\sigma_j(T, \Delta E) = 5\pi N_j Z_e^2 a_0^2 \alpha^2 \frac{I_H^2}{I_j^3} \frac{(T/I_j)^{\beta-1/2}}{4+(T/I_j)^{2\beta}} \times \exp\left(\frac{-\alpha \Delta E}{(I_j T)^{1/2}}\right), \quad (1)$$

in which $T \equiv E_p(m_e/M_p)$, in which E_p and M_p is the kinetic energy and mass of the projectile and m_e the electron mass, N_j the number of electrons in subshell j, Z_e is the effective charge number of the projectile, a_0 is the radius of the first Bohr orbit, I_j is the binding energy of subshell j, I_H is the binding energy of hydrogen: 13.6 eV and α and β are dimensionless constants of the order of unity. (See also the glossary at the end of this paper.)

Eq. (1) is valid for ionization by proton impact of both inner- and outer-shell electrons and is integrated over all impact parameters. It is applied by Rudd to describe measured energy distributions of electrons ejected by the impact of 10 to 50 keV protons in various gases. The constants α and β for the used gases [26] (N_2, O_2, Ne and Ar) are 0.91 and 0.75, respectively. We shall use eq. (1) with these values of α and β for a description of the inelastic energy loss of He^+ ions in the surface layers of the copper crystal. We thus assume that there is no qualitative difference between the differential ionization cross section for proton and for helium impact (at the same velocity). In fact, the latter cross section is 4 times larger if we assume that $Z_e = 2$. Furthermore, we assume the equation to be valid for copper atoms in a solid as well [+].

It will be convenient to rewrite the differential cross section $\sigma_j(T, \Delta E)$ as a product of N_j, the integral ionization cross section $\sigma_j^*(T)$ per electron, and the normalized kinetic energy distribution $f_j(T, \Delta E)$ of an ejected electron:

$$\sigma_j(T, \Delta E) = N_j \sigma_j^*(T) f_j(T, \Delta E), \quad (2)$$

where

$$\sigma_j^*(T) = 5\pi Z_e^2 a_0^2 \alpha^2 \frac{I_H^2}{I_j^2} \frac{(T/I_j)^{\beta}}{4+(T/I_j)^{2\beta}} \quad (3)$$

[+] Since copper is a conductor, eq. (1) cannot be used for the conduction electrons (i.e. the 4s-electrons).

and

$$f_j(T, \Delta E) = \frac{1}{\Gamma_j} \exp\left(\frac{-\Delta E}{\Gamma_j}\right), \quad (4)$$

in which Γ_j is the average kinetic energy of an ejected electron ($= (I_j T)^{1/2}/\alpha$). The average energy loss $\overline{\Delta E}_j$ of the projectile by ionization of an electron from subshell j is given by:

$$\overline{\Delta E}_j = I_j + \Gamma_j. \quad (5)$$

6.3. Impact-parameter dependence of the ejection probability

The integral ionization cross section per electron $\sigma_j^*(T)$ is equal to the probability $P_j(T, b)$ for a given electron to be ejected as a function of the impact parameter b of the collision, integrated over all impact parameters. In the following we shall assume, as before, that the ejection probability is constant for impact parameters smaller than a maximum b_m, and zero for impact parameters larger than b_m. Thus, for $b < b_m$ the ejection probability is given by eq. (3) divided by πb_m^2:

$$P_j(T, b) = 5Z_e^2\alpha^2 \frac{a_0^2}{b_m^2} \frac{I_H^2}{I_j^2} \frac{(T/I_j)^{\beta}}{4+(T/I_j)^{2\beta}} \equiv P_j(T) \quad \text{for } b \leq b_m$$

$$= 0 \quad \text{for } b > b_m. \quad (6)$$

Note that b_m is of the order of the radius (sub)shell j (see section 5.3).

The assumption that the impact-parameter dependence can be described by a step function is a simplification. It will, however, not substantially affect the comparison between theoretical and experimental energy losses.

6.4. Multiple ionization

If the ejection of an electron is independent of the simultaneous ejection of any other electron, then the total energy distribution of all ejected electrons can easily be obtained by a convolution of all individual energy distributions. Independence of the ionization probability of K- and L-shell electrons has been observed in various ion–atom collision experiments [52]. As far as we are aware, no such measurements have been performed for outershell electrons. Nevertheless, independence will be assumed in this case as well.

The convolution is performed easily if the most important ionizations (i.e. ionization of the 3p- and 3s-electrons, see table 4) are treated separately from the other ionizations and if the relatively small difference in binding energy and ejection probability of the 3s- and

3p-electrons are neglected. The subshells 3s- and 3p- will be denoted in the following by the index μ. Their weighted binding energy in the solid is denoted by I_μ (= 85 eV). The average kinetic energy Γ_μ of an ejected 3s- or 3p-electron is 45 eV. Thus, the average energy loss $\overline{\Delta E}_\mu$ by ionization of a 3s- or 3p-electron is 130 eV.

The convolution $f_\mu^{(k)}$ of k equivalent normalized kinetic energy distributions f_μ is (see eq. (4)):

$$f_\mu^{(k)}(T, \Delta E) = \frac{1}{(k-1)!}\frac{1}{\Delta E}\left(\frac{\Delta E}{\Gamma_\mu}\right)^k \exp\left(\frac{-\Delta E}{\Gamma_\mu}\right). \tag{7}$$

If mutual independence of the ejection probability $P_\mu(T)$ is valid and if differences between the 3s- and the 3p-subshell are neglected, then the probability $P_\mu^{(k)}(T)$ for the ejection of k electrons out of $N_\mu = 8$ electrons in the 3s- plus 3p-subshell, is given by a binomial distribution:

$$P_\mu^{(k)}(T) = \binom{N_\mu}{k} P_\mu^k (1 - P_\mu)^{N_\mu - k}. \tag{8}$$

The average number of ejected μ-electrons in a small-impact parameter collision is N_μ times the probability for one electron to be ejected, or: $8P_\mu(T)$.

The probability distribution $W_\mu^{(k)}(\Delta E_\mu)$ for an energy transfer of ΔE_μ from the ion to k ejected electrons from the μ-subshell is given by the product of eqs. (7) and (8):

$$W_\mu^{(k)}(\Delta E_\mu) = P_\mu^{(k)}(T) f_\mu^{(k)}(T, \Delta E_\mu - kI_\mu). \tag{9}$$

Note that the sum of the kinetic energies of the ejected μ-electrons is equal to the energy loss ΔE_μ of the ion minus k times the binding energy I_μ. The probability distribution $W_\mu(\Delta E_\mu)$ for an energy transfer ΔE_μ to any possible number of ejected μ-electrons is obtained by summation of $W_\mu^{(k)}$ over $k = 0$ to 8:

$$W_\mu(\Delta E_\mu) = \sum_{k=0}^{8} W_\mu^{(k)}(\Delta E_\mu). \tag{10}$$

Having treated the energy transfer to 3s- and 3p-electrons in this fashion, in a similar way the energy loss to the electrons in the other subshells (predominantly 3d- and 4s-electrons) is estimated by a convolution method.

The probability distribution W_i for energy transfer ΔE_i to all electrons of the atom in a small-impact parameter collision is:

$$W_i(\Delta E_i) = \int_0^{\Delta E_i} W_\mu(\Delta E_i - \Delta E_a) g(\Delta E_a)\, \mathrm{d}\Delta E_a, \tag{11}$$

in which $g(\Delta E_a)$ is the combined distribution function of the additional energy loss ΔE_a by excitation of any electron and by ionization of 3d-electrons. According to table 4, the average additional inelastic energy loss $\overline{\Delta E}_a$ is 120 eV, the spread σ_a is 45 eV. The energy loss distribution $W_i(\Delta E_i)$ in a collision with $b > b_m$, is given by $g(\Delta E_i)$ only. We have assumed that this distribution is independent of b.

6.5. Energy loss in more than one collision

We can apply eqs. (10) and (11) also to describe the energy loss distribution of ions after more than one small-impact parameter collision. In that case, k ranges from zero to N_μ times the number n_S of small-impact parameter collisions.

If the average number of ejected 3s- and 3p-electrons is larger than 1, the analysis is simplified by approximating the binomial distribution by a Poisson distribution:

$$P_\mu^{(k)}(T, n_S) \simeq \frac{\left(\bar{k}_\mu(n_S)\right)^k}{k!} \exp\left(-\bar{k}_\mu(n_S)\right), \tag{12}$$

in which $\bar{k}_\mu(n_S)$ is the average number of ejected 3s- and 3p-electrons in n_S small-impact parameter collisions. Since n_S is at most equal to the number of collisions n_C (which is in our experiment equal to $2\lambda - 1$; λ being the layer of backscattering) it follows that:

$$\bar{k}_\mu(n_S) = 8n_S P_\mu(T) \leqslant 8n_C P_\mu(T) = 8(2\lambda - 1) P_\mu(T), \tag{13}$$

The average energy loss $\overline{\Delta E}_\mu$ by ionization of 3s- or 3p-electrons is equal to:

$$\overline{\Delta E}_\mu = \bar{k}_\mu (I_\mu + \Gamma_\mu). \tag{14}$$

The spread in the number of ejected 3s- and 3p-electrons is equal to $\sqrt{\bar{k}_\mu}$. The spread σ_μ in the energy loss is then given by:

$$\sigma_\mu^2 = \bar{k}_\mu (I_\mu + \Gamma_\mu)^2 + \bar{k}_\mu \Gamma_\mu^2. \tag{15}$$

Note that the first term in eq. (15) results from the spread in the number of ejected electrons, the second term results from the spread in the kinetic energy of the ejected electrons.

With eqs. (7) and (9)–(12) we now derive the total inelastic energy loss distribution of a projectile as a function of backscattering layer λ, and of detection angle θ_s, by performing n_C convolutions of $g(\Delta E_a)$ with:

$$W_\mu(n_S, \Delta E_\mu) = \sum_k \frac{\left(\bar{k}_\mu E'\right)^k}{\Gamma_\mu^k} \frac{k}{E'(k!)^2} \times \exp\left(-\left(\bar{k}_\mu + \frac{E'}{\Gamma_\mu}\right)\right), \tag{16}$$

in which

$$E' \equiv \Delta E_\mu - kI_\mu, \tag{17}$$

and E' is the sum of the kinetic energies of k ejected 3s- and 3p-electrons.

In fig. 3 an example of the calculated energy distribution of backscattered 175 keV He^+ ions is shown. Only the energy loss by ionization of 3s- and 3p-electrons is taken into account. The backscattering angle is 90°, which corresponds to an elastic energy loss of 20.45 keV [$= (1 - k(90°))E_p$]. The inelastic energy loss distribution is calculated by use of eqs. (16) and (17). The effects of multiple scattering, of isotope differences, of excitations, of ionization of 3d-electrons and of polarization of the medium are not included. Curves A and B correspond to trajectories along which, on the average, two and five 3s- or 3p-electrons are ejected, respectively. The average inelastic energy loss is 260 and 650 eV, with a spread of 200 and 320 eV, respectively. Note that, if the average number of ejected 3s- or 3p-electrons is not too small, the energy distribution resembles a Gaussian function.

Since the number of additional inelastic loss processes is large ($\gg 1$) and the energy involved is small, the n_C convolutions of function $g(\Delta E_a)$ can be approximated [2] by one convolution with a Gaussian function with an average of $n_C\overline{\Delta E}_a$ and a spread of $\sqrt{n}_C\sigma_a$:

$$g^{(n_C)}(\Delta E_a) \simeq \frac{1}{\left(2\pi n_C\sigma_a^2\right)^{1/2}} \exp\left(\frac{-\left(\delta E_a - n_C\overline{\Delta E}_a\right)^2}{2n_C\sigma_a^2}\right). \quad (18)$$

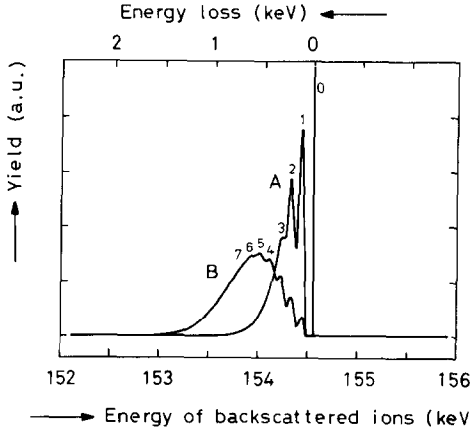

Fig. 3. The energy distribution of ions which are backscattered over 90° and have ejected, on the average, 2 (curve A) or 5 (curve B) 3s- and 3p-electrons of Cu atoms along the trajectory. (Other inelastic and elastic energy losses are neglected.) The energy loss per electron is equal to the mean binding energy (85 eV) plus the kinetic energy of the ejected electron. The energy loss distribution for k ejected electrons is obtained by k convolutions of the single-electron energy loss distribution. The total energy loss distribution is obtained by summation of the single distributions, each one weighted by its relative probability. The numbers refer to the average number of ejected electrons.

The average inelastic energy loss $\overline{\Delta E}_i$ is given by:

$$\overline{\Delta E}_i = \bar{k}_\mu(\lambda, \theta_s)\left(I_\mu + \Gamma_\mu\right) + n_C\overline{\Delta E}_a. \quad (19)$$

The spread σ_i in the inelastic energy loss is given by:

$$\sigma_i^2(\lambda, \theta_s) = \bar{k}_\mu(\lambda, \theta_s)\left(\left(I_\mu + \Gamma_\mu\right)^2 + \Gamma_\mu^2\right) + n_C\sigma_a^2. \quad (20)$$

7. Model for the peak shape

Because now the most important energy loss mechanisms are quantitatively known, we are able to derive a model for the shape of the surface peak in the energy spectrum of the backscattered ions at each detection angle θ_s, in our case 83°, 90° and 97°. The surface peak is the sum of the contributions of the two copper isotopes (labeled by κ), each one weighted by its natural abundance a_κ, and of all crystal layers (labeled by λ) each one weighted by its visibility V_λ. The contribution of each isotope and each layer is determined by the energy loss distribution of the ions which are backscattered from isotope κ in layer λ. The detection angle θ_s and multiple scattering determine the average elastic energy loss, see table 2. The average inelastic energy loss is related to the number n_C of collisions and to the average number n_S of small-impact parameter collisions.

The shape of each contribution is given by eqs. (16) and (17), convoluted with the distribution function of the (additional) inelastic energy losses (eq. (18)), convoluted with the resolution-function of the analyzer – which is assumed to be a Gaussian function – and, if necessary, shifted and broadened due to multiple scattering. The latter shifts and broadenings are also approximated by Gaussians. For simplicity, the various Gaussian convolutions are substituted by one shift and one Gaussian convolution. The shift is equal to the sum of the averages corresponding to the various Gaussian functions. The average of the substituted Gaussian function is zero, its width is the quadratic sum of the widths of the separate Gaussian functions.

If all contributions are added, one obtains the following equations between the shape of the normalized surface peak at detection energy E and detection angle θ_s [+]:

$$Y(E, \theta_s) = \sum_\kappa \sum_\lambda a_k V_\lambda(\theta_s) W_\mu(n_S, \Delta E_\mu), \quad (21)$$

$$E = k_\kappa(\theta_s)E_p - \left(\Delta E_\mu + n_C(\lambda)\overline{\Delta E}_a + \overline{\Delta E}_m(\lambda, \theta_s)\right), \quad (22)$$

in which $\overline{\Delta E}_m$ is the shift due to multiple scattering, $k_\kappa(\theta_s)$ is the kinematic factor for isotope κ and scattering angle θ_s.

[+] The normalization is performed by target-current integration and by comparison with a Bi-implanted standard.

Subsequently, $Y(E, \theta_s)$ is convoluted with a Gaussian function with an average of zero and a spread σ:

$$\sigma^2(\lambda, \theta_s) = n_C(\lambda)\sigma_a^2 + \delta_E^2 + \sigma_m^2(\lambda, \theta_s), \quad (23)$$

in which δ_E is the energy resolution of the analyzer (standard deviation is 270 eV) and σ_m is the spread in the ion energy caused by multiple scattering, see table 2.

The convoluted function $Y(E, \theta_s)$ is the theoretical, normalized height of the surface peak at analyzing energy E. The normalization is such that the area of the peak equals the number of visible atoms per row.

8. Comparison between the measured and calculated surface peaks

We have fitted the convolution of eqs. (21)–(23) to the measured surface peak at 83°, 90° and 97° detection angle in our experiment. Backscattering and detection probabilities are chosen as given in table 1. The magnitude of the shifts and the broadening by multiple scattering are chosen according to the results of the Monte Carlo calculation, table 2.

Free parameter in the fitting procedure is the average number $\bar{k}_\mu$ of ejected 3s- and 3p-electrons, or, which is equivalent (see eq. (19)), the average inelastic energy loss $\overline{\Delta E}_i$ as a function of the backscattering layer λ. Since the contributions of the third and deeper layers to the surface peak are relatively small, only the inelastic energy loss of ions backscattered in the first and in the second layer are varied independently. The inelastic energy loss of ions backscattered in deeper layers is assumed to be proportional to the difference in inelastic energy loss of ions backscattered in the first and in the second layer. The average additional inelastic energy loss $\overline{\Delta E}_a$ – by excitation, by ionization of 3d-electrons and by polarization of the medium – is taken according to the estimations given in table 4. Unfortunately, the primary energy E_p of the He ions is not known with sufficient accuracy. Therefore, E_p is taken as an additional free parameter in the fitting procedure.

The results of the fitting procedure are given in table 5 and are shown as solid curves in fig. 1 together with the experimental data. In the figure the contributions of the separate layers are shown as well. It is concluded that in one small-impact parameter collision, on the average, about 240 ± 30 eV kinetic energy of the ion is lost inelastically. This figure is slightly less than the estimation of 285 eV given in table 4. Regarding the uncertainty of about 25% in this estimation, the result is satisfying.

When the ion is backscattered in the second layer and detected at 90°, about three times as much energy is lost. When the ion is detected at 83° or 97°, the average inelastic energy loss is about 2.5 times as high. Note that after backscattering over 83° or 97°, the average impact parameter in the third collision is 30 pm, see table 2 and fig. 2.

Table 5
Average and spread of inelastic energy loss as a function of backscattering layer and detection angle. Figures are obtained by fitting model calculations for the surface peak to the measured surface peak. See fig. 1. The estimated error is about 20%

Scattering layer	Detection angle (deg)	Inelastic energy loss (eV)	
		average	spread
1	83	220	130
1	90	250	140
1	97	230	140
2	83	570	200
2	90	750	250
2	97	600	200

According to the stopping power data [20], an energy difference of 180 eV is expected between ions backscattered in the first and those backscattered in the second layer. This is 2.7 times lower than the energy difference resulting from our analysis.

The average number $\bar{k}_\mu$ of ejected 3s- and 3p-electrons in one small-impact parameter collision is 0.9 ± 0.2. The ejection probability $P_\mu(T)$ is, thus, 0.12 ± 0.03. Moreover, the results indicate that, if the impact parameter is larger than about 30 pm, almost no 3s- or 3p-electrons are ejected. These conclusions are in good agreement with the ejection probability P_μ as given in table 3 (weighted average is 0.14) and with the impact-parameter dependence of P_μ as described in section 6.3 *. Note furthermore that, according to eq. (6) and assuming an ejection probability of 0.12, the effective nuclear charge Z_c of the He^+ ion is 1.8.

In the fitting procedure, three independent values are found for the primary energy E_p of the ion beam. These values differ by less than 100 eV, which is negligible.

The spread σ_i in the inelastic energy loss as a function of the backscattering layer λ and detection angle θ_s follows from eq. (20). For example, the standard deviation in the energy loss of the ions which are backscattered in the first or in the second layer and detected at 90°, is 145 eV and 250 eV, respectively. The energy straggling (spread) of ions backscattered in the second layer, calculated by using Bohr's theory for straggling [2], is 160 eV. Calculated using the model of Chu [53], which usually gives better results, the strag-

* The probabilities given in table 3 are calculated for collisions in copper vapours. When the binding energy of the 3s- and 3p-subshell of a Cu atom in the solid is related to the Fermi level, the probabilities are about 20% higher. The value of the energy involved is about 10% lower.

gling would be less than 60 eV. Thus, also the usual formulas for straggling are not appropriate in our experimental setup.

9. Remarks

Not all effects which can influence the energy of the detected ions are included in our model for the surface peak. For instance, double ionization of the incoming He^+ ion can occur. However, He^{2+} is not detected in the analyzer. But if a He^{2+} ion recaptures an electron, its energy differs from that of an unchanged He^+ ion. The same holds for neutralization of the He^+ ion, followed by ionization. Furthermore, also excitation of He^+ can occur which could influence the kinetic energy of the ion. These effects are neglected, as they are assumed to be small.

The thermal velocity distribution of the Cu atoms from which the ions are backscattered, broadens the energy distribution of the detected ions. As this Doppler broadening is calculated to be only about 15 eV (standard deviation), this effect is almost negligible when compared with other broadening effects. Furthermore, the small spread in energy of the primary beam [54] is neglected as well, as it hardly affects our analysis.

It must be noted that the energy of the He^+ ions after backscattering is about 155 keV. Although not mentioned explicitly, this difference is incorporated throughout the performed calculations.

10. Summary and discussion

Comparison of the calculated shape of the surface peak with the shape in the measured energy spectra shows that the surface peak can be well described in terms of elastic and inelastic energy losses of the detected ions, if all main energy losses in each individual ion–atom collision in the surface layers are taken into account.

Analysis of the measured spectra reveals that the average inelastic energy loss of a 175 keV He^+ ion in a collision with a copper atom in a solid, with impact parameter smaller than the mean radius of the 3s- and 3p-subshell of Cu (26 pm), is about 240 eV. In a collision with a slightly larger impact parameter, the inelastic energy loss is only about 120 eV. Depending on backscattering layer and detection angle, the energy of the detected ions is also affected by multiple scattering. The effect has been evaluated by Monte Carlo computer simulations. It is found that, for ions backscattered in the second layer, the shift in energy by multiple scattering can be as much as a 200 eV, the spread (standard deviation) as much as 450 eV.

Energy loss of a He^+ ion by excitation or ionization of K- and L-shell electrons of Cu is very unlikely and can be neglected. If the impact parameter of the He^+ ion is as large as or smaller than the mean radius of the 3s- or 3p-subshell, data in the literature for electronic ionization- and excitation cross sections and our calculations indicate that, on the average, about 0.9 3s- or 3p-electrons are ejected. The corresponding average energy loss of the ion amounts to 120 eV. Furthermore, about 25 eV is lost by excitations to bound levels, and 50 eV by ionization and/or excitation of 3d- and 4s-electrons. Note that the latter processes depend only slightly on the impact parameter. Finally, 45 eV is lost continuously by polarization of the medium. The spread in the total inelastic energy loss in one small-impact parameter collision is about 145 eV. The value of the effective nuclear charge Z_e of the He^+ ion is found to be $+1.8$, which is larger than the effective charge Z''_{He} of $+1.5$ as given by the ratio of the He and the H stopping power in Cu at equal velocity [20].

Although the energy resolution of the analyzer and the effect of multiple scattering are comparable to the observed inelastic energy losses, it is concluded that the average electronic energy loss in small-impact parameter collisions is 2.5 to 3 times as high as calculated by using the tabulated data for the stopping power. This indicates a strong impact-parameter dependence of the electronic energy loss.

Of course, a high energy loss in a CHABLIS experiment increases the depth resolution. For instance, in our spectra the contributions of ions backscattered from the first and from the second layer can almost be separated. However, the relatively high value for the straggling, which is related to the high energy loss, dramatically reduces the depth resolution.

Note that, as a consequence of the mechanisms described above, the energy loss per unit of path length in the center of the crystal channels must be must less than the stopping power.

The impact parameter dependence of the energy loss has also been studied elsewhere in other experiments (such as channeling and/or transmission of ions through thin foils). However, since in those experiments the detected ions have had interactions at different values of impact parameter, the effect of the impact-parameter dependent energy loss will be smeared out. Finally, more insight into the energy losses of ions in the surface layers of a crystal can be obtained if an analyzer with a very high energy resolution were to be used; such an analyzer has been described, for instance, by Oku et al. [21]. Furthermore, energy measurements of backscattered ions in coincidence with secondary electrons or photons can lead to a better understanding of inelastic energy loss processes. Inelastic energy loss data of ion–atom collisions in metal vapours and gases are needed as well for a more complete description of the interaction of ions with atoms in solids .

We thank the FOM Institute for Atomic and Molecular Physics for the use of the medium-energy ion scattering facilities, and Dr. J.W.M. Frenken, Dr. J.F. van der Veen, Dr. F.H.P.M. Habraken, Dr. F.J. de Heer, Dr. A. Niehaus, Dr. M.E. Rudd and Dr. P. Sigmund for their help and suggestions.

Glossary

a_0	Bohr radius (52.9 pm),
b	impact parameter of the collision,
b_m	maximal impact parameter for which ionization can occur,
E_p	primary energy of the ions,
$f_j(T, \Delta E)$	kinetic energy distribution of electrons ejected from subshell j,
$f_j^{(k)}(T, \Delta E)$	total kinetic energy distribution of k electrons ejected from subshell j,
$g(\Delta E_a)$	distribution function of additional inelastic energy losses,
I_j	binding energy of subshell j,
I_H	binding energy of hydrogen (13.6 eV),
$k_\kappa(\theta_s)$	kinematic factor for isotope κ and scattering angle θ_s,
k_μ	number of ejected μ-electrons,
m_e	electron mass,
M_p	mass of projectile,
n_C	number of collisions of the ion in the solid,
n_S	number of small-impact parameter collisions of the ion in the solid,
N_j	number of electrons in subshell j,
P_j	probability for the ejection of a given electron in subshell j,
r_j	radius of subshell j,
T	$\equiv E_p(m_e/M_p)$,
V_λ	visibility of layer λ,
$W_j(\Delta E_j)$	probability distribution for an energy transfer ΔE_j to the electrons in subshell j,
$Y(E, \theta_s)$	(normalized) spectrum yield at energy E and detection angle θ_s,
Z_e	effective charge of the ion,
α	dimensionless constant ($= 0.91$),
β	dimensionless constant ($= 0.75$),
δ_E	energy resolution of the analyzer,
ΔE_a	additional inelastic energy loss (i.e. loss not due to 3s- or 3p-electrons),
ΔE_i	inelastic energy loss
ΔE_m	elastic energy loss due to multiple scattering,
δ_θ	deflection in the trajectory of the ion with respect to its initial direction,
ΔE	kinetic energy of ejected electrons,
Γ_j	average kinetic energy electrons ejected from subshell j,
λ	number of the layer of backscattering,
μ	index indicating the 3s- and 3p-subshell of Cu,
σ_a	spread in the additional inelastic energy loss,
σ_m	spread in the elastic energy loss,
$\sigma_j(T, \Delta E)$	differential ionization cross section of subshell j,
$\sigma_j^*(T)$	integral ionization cross section of subshell j,
θ_s	angle between primary beam and analyzer (= detection angle).

References

[1] N. Bohr, Philos. Mag. 25 (1913) 10.
[2] N. Bohr, K. Dan. Vidensk. Selsk. Mat. Fys. Medd. 18 (1948) no. 8.
[3] J. Lindhard, K. Dan. Vidensk. Selsk. Mat. Fys. Medd. 28 (1954) no. 8.
[4] J. Lindhard and M. Scharff, K. Dan. Vidensk. Selsk. Mat. Fys. Medd. 27 (1953) no. 15.
[5] E. Bonderup, K. Dan. Vidensk. Selsk. Mat. Fys, Medd. 35 (1967) no. 17.
[6] J.F. Ziegler, Helium Stopping Powers and Ranges in all Elements (Pergamon, New York, 1978).
[7] R.J. Culbertson, S.P. Withrow and J.H. Barrett, Nucl. Instr. and Meth. B2 (1984) 19.
[8] E. Bøgh, Radiat. Eff. 12 (1972) 13.
[9] W.F. van der Weg, H.E. Roosendaal and W.H. Kool, Radiat. Eff. 17 (1973) 91.
[10] E.J. van Loenen, A.E.M.J. Fischer, J.F. van der Veen and F. Legoues, Surf. Sci. 154 (1985) 52.
[11] J.C. Eckardt, G.H. Lantschner, M.M. Jakas and V.H. Ponce, Nucl. Instr. and Meth. B2 (1984) 168.
[12] H. Geissel, W.N. Lennard, H.R. Andrews, D. Ward and D. Phillips, Phys. Lett. 106A (1984) 371.
[13] H.S. Jin and W.M. Gibson, Nucl. Instr. and Meth. B13 (1986) 76.
[14] P. Mertens and T. Krist, Nucl. Instr. and Meth. B13 (1986) 95.
[15] P. Sigmund and K.B. Winterbon, Nucl. Instr. and Meth. B12 (1985) 1.
[16] W.N. Lennard, D. Phillips, I.V. Mitchell, H.R. Andrews and D. Ward, Nucl. Instr. and Meth. B2 (1984) 116.
[17] T. Krist, P.J. Scanlon, P. Mertens, K.M. Barfoot, I. Reid and C.Y. Cheng, Nucl. Instr. and Meth. B14 (1986) 179.
[18] J.W.M. Frenken and J.F. van der Veen, Phys. Rev. Lett. 54 (1985) 134.
[19] P.F.A. Alkemade, W.C. Turkenburg and W.F. van der Weg, Nucl. Instr. and Meth. B15 (1986) 126.
[20] J.F. Ziegler, J.P. Biersack and U. Littmark, The Stopping and Range of Ions in Solids (Pergamon, New York, 1985).
[21] T. Oku, J. Kanasaki, N. Matsunami, N. Itoh, K. Matsuda and M. Aoki, Nucl. Instr. and Meth. B15 (1986) 142.
[22] O.S. Oen and M.T. Robinson, Nucl. Instr. and Meth. 132 (1976) 647.
[23] P.F.A. Alkemade, Thesis, Utrecht (1987) 25.
[24] I. Nagy, J. László and J. Giber, Nucl. Instr. and Meth. B15 (1986) 8.

[25] H.H. Mikkelsen and P. Sigmund, to be published.
[26] M.E. Rudd, Phys. Rev. A20 (1979) 787.
[27] W.E. Wilson, L.H. Toburen and W.A. Glass, Radiat. Res. 63 (1975) 387.
[28] D.J. Bierman and D. van Vliet, Physica 57 (1972) 221.
[29] R. Haight and L.C. Feldman, T.M. Buck and W.M. Gibson, Nucl. Instr. and Meth. B2 (1984) 501.
[30] G.G. Ross and B. Terreault, Nucl. Instr. and Meth. B15 (1986) 146.
[31] R.G. Smeenk, R.M. Tromp, H.H. Kersten, A.J.H. Boerboom and F.W. Saris, Nucl. Instr. and Meth. 195 (1982) 581.
[32] W.C. Turkenburg, H.H. Kersten, B.G. Colenbrander, A.P. de Jongh and F.W. Saris, Nucl. Instr. and Meth. 195 (1976) 271.
[33] J.W.M. Frenken, private communication.
[34] J.F. van der Veen, Surf. Sci. Rep. 5 (1985) 199.
[35] H.L. Davis and J.R. Noonan, J. Vac. Sci. Technol. 20(3) (1982) 843.
[36] B.R. Appleton and G. Foti, in: Ion Beam Handbook for Material Analysis, eds., J.W. Mayer and E. Rimini (Academic Press, New York, 1977) 67.
[37] W.K. Chu, J.W. Mayer and M.A. Nicolet, Backscattering Spectroscopy (Academic Press, New York, 1978).
[38] A comprehensive overview is: H.S.W. Massey, E.H.S. Burhop and H.B. Gilbody, Electronic and Ionic Impact Phenomena, 2nd ed. (Clarendon, Oxford, 1974).
[39] J. Lindhard and A. Winther, K. Dan Vidensk. Selsk. Mat. Fys Medd. 34 (1964) no. 4.
[40] F.J. de Heer, J. Schutten and H. Moustafa, Physica 32 (1966) 1793.
[41] M.E. Rudd, R.D. DuBois, L.H. Toburen, C.A. Ratcliffe and T.V. Goffe, Phys. Rev. A28 (1983) 3244.
[42] D.E. Johnson, G. Basbas and F.D. McDaniel, Atom. Data and Nucl. Data Tables 24 (1979) 1.
[43] M. Gryzinski, Phys. Rev. 138 (1964) A 1268.
[44] J.M. Hansteen, O.M. Johnsen and L. Kocbach, Atom. Data and Nucl. Data Tables 15 (1975) 305.
[45] M. Barat and W. Lichten, Phys. Rev. A6 (1972) 211.
[46] K.D. Sevier, Atom. Data and Nucl. Data Tables 24 (1979) 323.
[47] D.D. Cohen and M. Harrigan, Atom. Data and Nucl. Data Tables 33 (1985) 255.
[48] P. Richard, in: Atomic Inner-Shell Processes, ed., B. Crasemann, vol. 1 (Academic Press, New York, 1975).
[49] J.M. McGuire and P. Richard, Phys. Rev. A8 (1973) 1374.
[50] E.S. Solov'ev, R.N. Il'in, V.A. Oparin and N.V. Fedorenko, Sov. Phys. JETP 15 (1962) 459.
[51] A. Dalgarno, in: Atomic and Molecular Processes, ed., D.R. Bates (Academic Press, New York, 1962).
[52] J.H. McGuire and L. Weaver, Phys. Rev. A16 (1977) 41.
[53] W.K. Chu, Phys. Rev. A13 (1976) 2057.
[54] W.C. Turkenburg, W. Soszka, F.W. Saris, H.H. Kersten and B.G. Colenbrander, Nucl. Instr. and Meth. 132 (1976) 587.